Glow discharge in low pressure plasma PVD: mathematical model and numerical simulations

A. Speranza, A. Monti

Industrial Innovation Through Technological Transfer – I^2T^3 Onlus

alessandro.speranza@i2t3.unifi.it

L. Barletti, I. Borsi, L. Meacci

Dip. di Matematica "U. Dini" Università degli Studi di Firenze

S. Fanfani

Galileo Vacuum Systems srl, Prato

December 14, 2010

Abstract

In this paper we analyze the problem of glow discharge in low pressure plasma in industrial plant, for chambers of different shapes and various working parameters, like pressure and electric potential. The model described is based upon a static approximation of the AC configuration with two electrodes and a drift diffusion approximation for the current density of positive ions and electrons. A detailed discussion of the boundary conditions imposed is given, as well as the full description of the mathematical model.

Numerical simulations were performed for a simple 1D model and two different 2D models, corresponding to two different settings of the industrial plant. The simpler case consists of a radially symmetric chamber, with one central electrode (cathode), based upon a DC generator. In this case, the steel chamber acts as the anode. The second model concerns a two dimensional horizontal cut of the most common plant configuration, with two electrodes connected to an AC generator. The case is treated in a "quasi-static" approximation. The three models show some common behaviours, particularly including the main expected features, such as dark spaces, glow regions and a wide "plasma region". Furthermore, the three shown models show some similarities with previously published results concerning 1D and simplified 2D models, as well as with some preliminary results of the full 3D case.

keywords: PVD, glow discharge, surface coating, plasma, drift-diffusion

1 The industrial problem

Plasma PVD (Physical Vapour Deposition) is a widely used process, applied for, particularly, in the coating industry. The process basically aims at forming a thin coating layer on the surface of different substrates. PVD is normally used as an alternative physical process to classical wet chemical process, such as galvanic baths.

The case we particularly refer to concerns the metalization of plastic headlights for automotive (Fig. 1), with a thin aluminium layer, and its coating with thin polymeric film, such as HMDSO (Hexa Methyldisiloxane). The HMDSO is used to protect the metalization from external agents and ageing.

As it can be seen from Fig. 1-b, the industrial plant consists of three main parts. The two semi-chambers visible at the bottom of the figure, contain the headlights to be processed. The two moving parts close alternatively on the fixed part of the plant (rectangular in Fig. 1-b) as shown in the photograph (Fig. 1-a). In this configuration, the two moving semi-chambers contain circular plates disposed all around the axis of symmetry, moving in planetary motion. The headlights are deposed on the plates during the process. The fixed part of the plant, visible as rectangle at the top of Fig. 1-b, contain the electrodes (see below) and the vacuum pump with all the pipelining. The industrial plant is normally made in two different configurations. The configuration represented in figure, has two cylindrical vertical electrodes and works on alternate current (AC), *i.e.*, an alternate electric field is applied to the electrodes in order to produce the glow discharge. In the second configuration, one cylindrical electrode (normally the cathode) is located in the center of the chamber and a direct electric potential (DC) is applied to it. In this second configuration, the metallic chamber itself works as the anode.

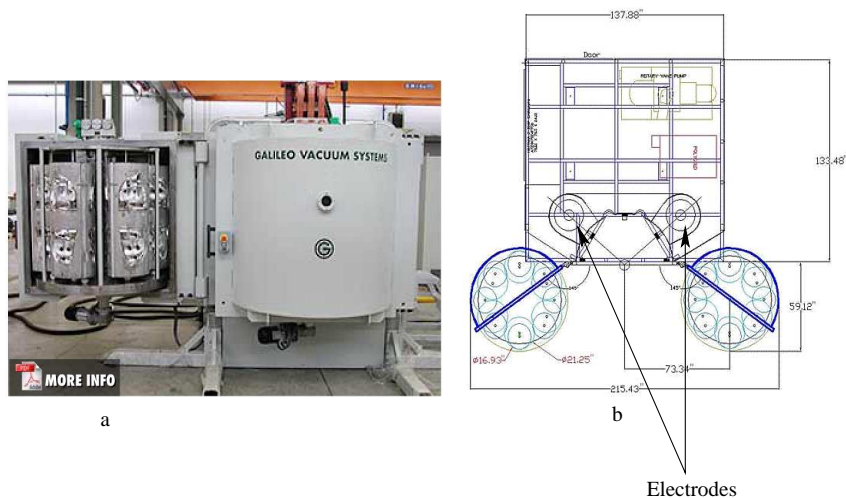The industrial process proceeds through three main steps

Figure 1: a) Photograph of the industrial plant by Galileo Vacuum Systems s.p.a., objecto of the work. The headlights on the left hand side, have been already exposed to metalization, while the semi-chamber on the right hand side is closed and the process is active. b) Schematic representation of the PVD chamber (not the one produced by Galileo Vacuum Systems) as seen from the top. The chamber has two semi-chambers which can contain the headlights to treat, deposed on circular plates. The rectangular part above the two semi-chambers contains the electrodes and the vacuum pump.

- Vacuum: one of the two mobile semi-chambers is locked against the fixed part, and vacuum ($\sim 10^{-3}$ mbar) is made

- Metalization: aluminium filaments located all along the height of the mobile semi-chamber are heated via Joule effect. In such a low pressure atmosphere, aluminium vaporizes and a thin layer of metallic aluminium deposits onto the headlights surface. The more uniform and denser is the cloud of vaporized aluminium, the more uniform and thicker will be the metallic layer on the surface.

- Polymer coating: a strong electric potential difference ($\sim$ 2-5 kV) is applied to the electrodes. In these conditions, the residual atmosphere transforms into plasma and a glow discharge appears. At the same time, a monomer flows through nozzles within the chamber, increasing the pressure up to 1-5×10^{-1} mbar. The plasma atmosphere induces the polymerization on the substrate of the headlights, and a thin polymer film covers the aluminium layer.

In this work, we will neglect completely the first two steps of the process, and will concentrate on the third one. In particular, we will concentrate on the part in which, in low pressure atmosphere, the electric potential is applied to the electrodes (or to the cathode, in the configuration with one central electrode) and the glow discharge is induced [6, 11, 18, 21, 22, 28], while the monomer flows and polymerization occurs. The aim of our work is to model the glow discharge process, in order to gain information concerning, *e.g.*, the distribution of positive and negative charges, or the electric field within the chamber, during the glow discharge. It is clear, in fact, that HMDSO polymerizes under the influence of the plasma atmosphere. However, it is not clear in what particular conditions the polymerization is actually favored. In other words, our final aim is to describe the plasma atmosphere all across the chamber, in order to correlate its features, with the main features of the resulting polymer film, such as thickness, homogeneity etc. With this information, one could try to optimize the shape of the chamber and the value of the main process parameters, in order to have the best possible result, in the widest part of the chamber.

2   The physical and mathematical model

As mentioned in the previous section, this work focuses on the final step of the industrial process, *i.e.*, on the polymerization of the HMDSO in low pressure plasma. In fact, our model concerns more the plasma atmosphere in which the HMDSO polymerizes, rather than the process of polymerization itself. The polymerization would be rather difficult to model, as the process is strongly influenced by different factors, not least the substrate on which the polymer film is formed or its shape, besides the conditions of the plasma itself (see,

for instance, [17, 19]). For all these reasons, given that a realistic model of polymerization would be rather difficult to achieve, and even more complex to solve numerically (due to the strongly asymmetric geometry of the domain), we focus on the analysis of the conditions in which the monomer polymerizes while flowing across the chamber. Our final aim is to describe the conditions of the plasma, in terms of electric field, density distribution of positive and negative charges etc., in order to correlate these conditions with the main features of the obtained polymer film.

2.1 Hypotheses of the model

Our mathematical model is based upon a set of simple assumptions, aimed at simplifying the set of equations and, in parallel, the geometry of the domain. As far as the chamber is concerned, we therefore assume

- The steel chamber is perfectly cylindrical.

- The electrodes (one or two, depending on the configuration of the plant) are perfectly cylindrical and not connected anyhow to the chamber. In other words, the electrodes "float" in the chamber, as they are generally shorter than the chamber itself.

In order to simplify the set up of the mathematical model, we then make the following assumptions, concerning the plasma atmosphere:

- Thermal (and thermodynamic) equilibrium is assumed throughout the chamber. In this way, we assume a perfectly static atmosphere.

- Plasma is made only of two species of charged particles: positive single ionized atoms (ions) and free electrons. Clearly this assumption is rather strong, especially in the final part of the process, *i.e.*, when the monomer is flowing within the chamber and the polymer film is forming. When this happens, the atmosphere is made of a great number of species, such as monomers, ions, radicals, pieces of polymer chains and so on, however, this is the only possible starting point for any kind of modelling approach.

- We always consider a stationary electric field, even in the case of an alternate potential difference applied to the electrodes. In this way we can neglect all the terms involving the variation of the electric field in the Maxwell equations (see below).

Moreover, we will make a further assumption, concerning, as we will see in later sections, the boundary conditions to impose to our set of equations: we assume that all the steel parts composing the chamber and the electrodes, are "perfectly absorbing", *i.e.*, all the charged particles hitting the surface of any steel part, go back into the chamber as neutral particles. In other words, charged particles are never reflected into the chamber, as they are.

Before proceeding to the description of the mathematical model, let us go back for a moment to the assumption of a static electric field mentioned earlier, in spite of the choice of the chamber configuration with one (DC generator) or two (AC generator) electrodes. In fact, this assumption is reasonable, as, even in the case of two electrodes, the frequency of the applied field is of the order of 100 kHz. Given that the radius of the chamber is normally of the order of 1 m, and that the wavelength of the applied field is of the order of 3 km, it turns out that, within the extension of the chamber, the electric field can be considered uniform. In other words, the chamber is sufficiently small to allow us the use of a "quasi-static approximation", *i.e.*, to neglect all the possible delay effects due to the variation of the electric field within it.

As we will shortly see in the following sections, in spite of the drastic simplifications of the physical problem that we made in order to solve numerically the mathematical model, our results turn out to correlate fairly well with observations and direct measures. In fact, although the real atmosphere consists of many types of ions and radicals, resulting from the polymerization process, observations show, as in simpler atmosphere, the formation of a "dark space" surrounding the electrodes, confined by a bright region: "the glow". As we will see in the following sections, in our numerical results the two regions are clearly evident. The two regions differ in particular in the values of the number density of charged particles and electric field intensity. In other words, in spite of the high degree of approximation of our model, our numerical results turn out to give some reasonable insights of the actual problem, marking an important step forward in the interpretation of observations and direct measures, aimed at the optimization of the industrial setting.

2.2 Set up of the equations

Once the physical model has been set as described in the previous section, the set of equations to solve turns out to be rather simple. As mentioned, we assume a steady atmosphere and thermal equilibrium across the chamber. Furthermore, we assume a steady electric field applied to the electrodes. In these hypotheses, the electric potential must obey the non homogeneous Poisson equation, *i.e.*,

$$\Delta V = -\frac{e}{\epsilon}(n_i - n_e) \qquad (1)$$

where Δ is the Laplace operator, V is the electric potential, e is the electron electric charge ($\simeq 1.6\,10^{-19}$ C),

3

ϵ is the absolute dielectric constant of the atmosphere and n_i, n_e are the number densities of ions and electrons respectively. For the equation above, one must set boundary conditions which, in this case, turn out to be straightforward Dirichlet boundary conditions, as it will be shown in the following section.

As far as ions and electrons current densities $\mathbf{J_{i,e}}$ are concerned, in the hypothesis of a continuous model (see below), they obviously must obey the stationary continuity equation, *i.e.*,

$$\nabla \cdot \mathbf{J_i} = \mu_e n_e S(V) \tag{2}$$
$$\nabla \cdot \mathbf{J_e} = \mu_e n_e S(V) \tag{3}$$

where μ_e is the electrons mobility coefficient and $S(V)$ is the ionization frequency, which is obtained from the Townsend formula [5, 35, 39]

$$S(V) = A \exp\left\{ -B \left(\frac{P}{|\nabla V|} \right)^{0.4} \right\} P \, |\nabla V| \tag{4}$$

The term on the right hand side of Eqs. (2,3), $\mu_e n_e S(V)$, basically expresses the number density of ion/electron pairs formed through a collision between a neutral particle and a free electron, per unit time. As obvious, this term depends on the pressure P and the electric field module $|\nabla V|$. Note that, compared to the standard notation (*e.g.*, [5, 28]), we pulled the electron mobility out of the definition of the Townsend coefficient, in order to make the typical scaling of the equations more evident. The two coefficients A and B in the equation above, are obtained by a fit of experimental data, and depend on the composition of the atmosphere (see, *e.g.*, [24, 29, 30, 35, 39]). Typical values of the two coefficients range between 4 and 60 cm^{-1} Torr^{-1}, for A, and between 14 and 36 (V/cm Torr)$^{0.4}$, for B. In the following, we made a fairly conservative choice, in order to control more easily the numerical calculations and used A between 2 and 3 cm^{-1} Torr^{-1} and B between 12 and 13 (V/cm Torr)$^{0.4}$, comparable with the values for He reported by Ward [39] and with the values used by Boeuf and Pitchoford [5]. As shown in Fig. 2, the first Townsend coefficient is strongly dependent on the choice of the set of coefficients A and B. However, as the electric field grows, and $S(V)/P|\nabla V|$ settles on a constant value, the frequency of ionization $S(V)\mu_e$ becomes linear with $|\nabla V|$.

The current density $\mathbf{J_q}$ of charged particles q (i or e) in Eqs. (2,3) is modeled through a simple drift-diffusion equation, *i.e.*,

$$\mathbf{J_q} := -\mathrm{sgn}(q)\mu_q n_q \nabla V - D_q \nabla n_q \tag{5}$$

where D_q is the diffusivity coefficient and is linked to the charge carrier mobility via the so called Einstein's formula

$$D_q = \frac{\kappa_{\mathrm{B}} T_q}{e} \mu_q$$

where κ_{B} is the Boltzmann constant, and T_q is the temperature of the charged particle. In the following, we made the assumption that ions are in thermal equilibrium with the neutral gas, therefore $T_i = T = 300$ K, while the electron temperature was set to $T_e = 10000$ K throughout our domain, corresponding to an average energy $E_e \sim 0.4$ eV. The electrons and ions mobility are taken, coherently with the choice we made for the first Townsend coefficient, as $\mu_e = 1333$ m^2 V^{-1}s^{-1} ($\mu_e P = 10^6$ cm^{2}V^{-1}s^{-1}Torr) and $\mu_i = 10.66$ m^2 V^{-1}s^{-1} ($\mu_i P = 8 \times 10^3$ cm^{2}V^{-1}s^{-1}Torr) respectively, at a pressure of 10 Pa, as reported by Ward [39].

Our set of equations therefore consists of Eqs. (1)-(2) and (3), with the use of (5), in the three unknowns V, n_i and n_e.

2.3 Comments on the model

As shown, our model is based upon the heuristic assumption, to be verified *a posteriori*, that a fluid model is suitable throughout the whole domain. Clearly, this assumption will have to be checked against the parameters used to define the conditions of our plasma. It is, in fact, well known, that in a very low pressure plasma a collision-free sheath could be formed in contact with an absorbing or a neutral wall [7, 34], effectively confining the neutral plasma. As the hypothesis of high collisionality is not satisfied, a continuous model may not be applicable to this case. Within the sheath region, electrons are almost absent and $n_i \gg n_e$. Furthermore, the sheath is confined by a transition region (the pre-sheath) where the plasma is almost exactly neutral (*i.e.*, $n_i \simeq n_e$). The sheath is stable when the so called *Bohm criterion* is satisfied, *i.e.*, when the ions drift velocity is larger than some critical speed, corresponding, as shown later [1, 2], to a Mach surface for the ions flux. As mentioned, when the conditions for the formation of the sheath are satisfied, a purely continuous model cannot be used, as the assumption of high collisionality is not satisfied within the sheath and the pre-sheat. In this case, one possible approach is to develop a fluid model that connects, in the limit, with the sheath model (see, *e.g.*, [12, 38]). However, the conditions for the formation of a stable sheath are not completely clear yet. It was shown that the Bohm criterion results, in fact, in a sufficient but not necessary condition for the sheath formation [27, 36]. It was also shown by Valentini [36] and Riemann [27], that such a criterion has to be strongly modified when collisions are present. In other words, a sheath could be formed even in collisional plasma, although its characteristics are quite different in this case. Godyak and Sternberg [13] showed that the model upon which the formation of
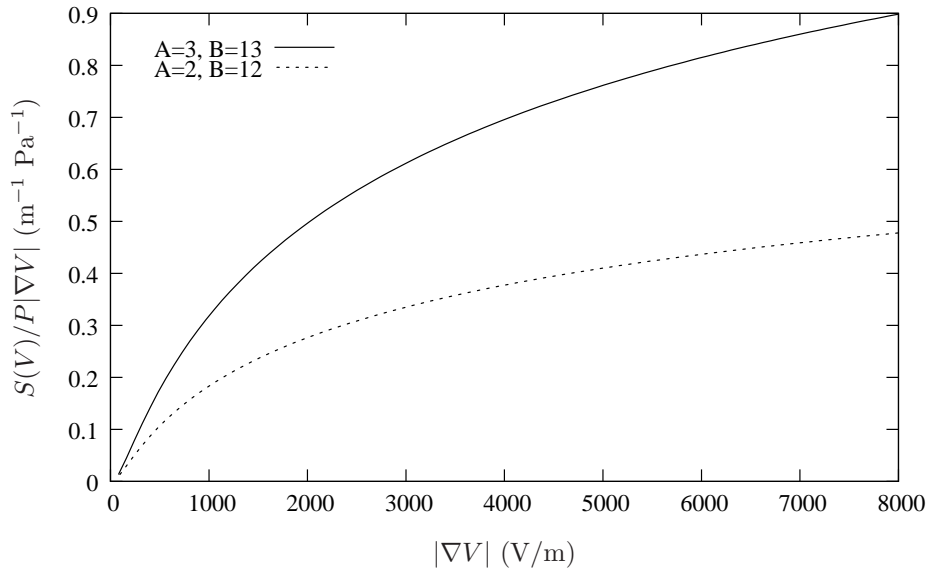
Figure 2: First Townsend coefficient rescaled by pressure and electron mobility as defined in Eq. (4), as a function of $|\nabla V|$. The two sets of coefficients $A = 2 - 3$ cm^{-1} Torr^{-1} and $B = 12 - 13$ (V/cm Torr)$^{0.4}$ correspond roughly to the data published in [39] for He.

such a sheath is described, is intrinsically inconsistent, suggesting that a modification on the basic assumptions should be made. Valentini [37], on the other hand, showed that in a discharge plasma, *i.e.*, a slightly ionized, low pressure plasma, similar to ours, the sheath can still be formed, under appropriate conditions. However, the whole sheath concept, in particular in front of the cathode, should be somehow redefined. In fact, in these conditions, a fluid model can usually be used throughout the whole domain, as collisions are frequent and important, even though, the electrode fall still region turns out to show very peculiar characteristics, compared to the neutral plasma region. In order to take into account of the peculiar behaviours of that region, authors chose to use different methods. Hagelaar et al., for instance [18], used boundary conditions to take into account of the different behaviour of the fast electrons generated within the cathode fall region. Surendra et al. [33], coupled a fluid model (similar to ours) with another model for the fast electrons. On the other hand, other authors [4, 6, 11, 14, 15, 20, 25, 28, 31, 40] used a fluid model throughout the whole domain, investigating its range of applicability, and choosing boundary conditions in order to have a tractable and yet physically meaningful model. Boeuf and Pitchford [5] argued that a fluid drift-diffusion model can normally be used with values of the pressure of the order of 100 mTorr (~ 13 Pa). In fact, the same approach was also used for RF glow discharge models [3, 4, 15, 16, 23, 25], as long as the number of collisions remains high enough, *i.e.*, as long as the applied pressure is sufficiently high. The

threshold value for the pressure normally grows from 100 to 500 mTorr (~ 67 Pa), for applications of the fluid model to an RF discharge model. However, the argument, in both cases, the AC and DC, is based upon the fact that, for pressures above some values, the ions mean free path is normally the smallest length scale, compared to, for instance, the electrons Debye length, the typical length scale of the model, and so on. In these conditions, collisions can be considered frequent enough to allow for a continuous model to be physically meaningful.

A similar argument applies exactly also to our case. As mentioned above, we chose a pressure value of 10 Pa (~ 75 mTorr), which is very close to the lowest value mentioned, for instance by Boeuf and Pitchford [5]. In these conditions, the ions mean free path λ_i turns out to be of the order of 1 mm. This value should be compared with the typical length scale of the chamber ($L = 1$ m) and, for instance, the electrons Debye length λ_D. In our case, the electrons Debye length turns out to be $\lambda_D = L/\sqrt{\tilde{T}_e/\tilde{n}_e}$, where $\tilde{T}_e = T_e/T$ and $\tilde{n}_e$ is the non dimensional electrons number density (see next section). Since we set $\tilde{T}_e \sim 30$ and from our numerical results, we have at most $\tilde{n}_e \sim 10^6$, we get that $\lambda_D > 10$ mm. In any case, near the electrodes, where $\tilde{n}_e$ decays down to 10^3, we have $\lambda_D \sim 0.1$ m. This particular result indicates [26] that the electric field may not be strong enough to confine the ions in a very narrow region in contact with the electrode. Instead, collisions allow the ions to diffuse further inside the bulk region. This general consideration is supported by our numer-

5

ical results. As we will see in the following sections, the cathode sheath region, shows a dominance of ions, as it should be, but a still large presence of electrons ($n_e > 10^8$ m^{-3}). Furthermore, our sheath is confined by a region with a high net charge density, and not by a neutral region such as the one assumed to confine the sheath region in the collision-less plasma. In fact, as already predicted by Valentini [37], in our case, the net charge density reaches a maximum before decaying rapidly to zero in the neutral plasma region, coherently with the assumption of a highly collisional plasma. Sheridan and Goree [32] showed that the non-collisional and the collisional regimes connect smoothly through an intermeidate regime with the relavant index being, once again, the collision parameter $\alpha = \lambda_{\mathrm{D}}/\lambda_i$. The authors argued that the collisional regime extends in the region $\alpha > 0.1$. For values of α of the order 10, like in our case, the regime is already highly collisional and the fluid model should be fully acceptable.

In spite of the low pressure, we therefore conclude that our plasma shows a still strongly collisional regime that allows us, although close to the limiting case, to use a continuous model throughout the domain. However, even when a smooth connection between the the numerical results of the fluid model and an asymptotic analysis of the boundary layer was attempted [38], the two solutions showed an appreciable difference only at a very short length-scale which are far beyond our aims. Clearly, the argument of high collisionality applies only since we chose to focus on the final step of the industrial process (that we referred to as "Polymer coating" in Sec. 1). The pressure there grows rapidly between 10^{-3} mbar to 0.1-0.5 mbar as the monomer flows through the chamber and polymerization occurs. The same argument, on the other hand, would not apply if we wanted to describe the conditions of the plasma atmosphere at the very start of the process, *i.e.*, when the pressure is still 100 times lower, and the atmosphere consists only of the residual air present in the chamber.

3   The problem of boundary conditions

To the set of equations described in the previous section, one has to impose boundary conditions on each one of the steel parts which confine the problem domain, *i.e.*, the two electrodes and the chamber surface. As mentioned in the previous section, to the Poisson equation for the electric potential Eq. (1), one can simply impose Dirichlet boundary conditions. For instance, defining V_C, the potential of the steel chamber, as the reference potential, and redefining all the potentials as potential differences $\tilde{V} = V - V_C$ and swapping

V and $\tilde{V}$, we can set

$$
\begin{aligned}
V &= & V_0 & \quad \text{on the anode} \\
V &= & -V_0 & \quad \text{on the cathode} \\
V &= & 0 & \quad \text{on the steel chamber}
\end{aligned}
\tag{6}
$$

In this way, the potential difference between the two electrodes is set to be $2V_0$. The potential difference with the chamber is, respectively, V_0 and $-V_0$ for the anode and the cathode.

There is no such a simple way to express boundary conditions for the number densities n_i and n_e, unless we make some further assumptions on the actual interaction between charged particles and the electrodes or the chamber. Let us therefore analyze the condition to impose on the different parts of the plant, for the two species of charged particles. For the ions following, *e.g.*, the arguments by Hagelaar et al. [18], one can make the following assumptions:

- The cathode absorbs ions, in the sense that any ion hitting the cathode surface, captures a free electron emerging on the surface and is reflected into the chamber as a neutral particle. We assume, as mentioned earlier, that the cathode is a "perfect absorber of ions" in the sense that none of the ions hitting the surface is simply reflected into the chamber. In these conditions, the density flux $\mathbf{J_i}$ reduces to just the drift term, while the diffusion vanishes, *i.e.*, we set a simple Neumann boundary condition such as

$$
\nabla n_i \cdot \boldsymbol{\nu} = 0
\tag{7}
$$

  where $\boldsymbol{\nu}$ is the normal versor pointing inward the cathode surface (*i.e.*, outwards from our domain)

- The anode does not emit (or absorb) ions, thus the net inward flux across its surface must vanish. In other words, on the anode we set a mixed boundary condition of the type

$$
-\mathbf{J_i} \cdot \boldsymbol{\nu} := -(-\mu_i n_i \nabla V - D_i \nabla n_i) \cdot \boldsymbol{\nu} = 0
\tag{8}
$$

  where $\boldsymbol{\nu}$ is the normal versor pointing inward the anode surface (*i.e.*, outwards from our domain)

- Following this argument, the steel chamber will have to behave in a way which is similar to the anode or the cathode, depending on the direction of the electric field (and thus, of the ions flux). When the electric field $-\nabla V$ "enters" the surface, *i.e.*, has the same sign as the outwards normal versor, the steel chamber behaves like a cathode. On the other hand, when the electric field $-\nabla V$ is outward the surface, *i.e.*, entering our domain, and therefore anti-parallel to the outward normal ver-

sor, the steel chamber behaves like the anode. In compact form, we can write this condition as

$$
\begin{aligned}
\mathbf{J_i} \cdot \boldsymbol{\nu} &:= (-\mu_i n_i \nabla V - D_i \nabla n_i) \cdot \boldsymbol{\nu} = \\
&= -a_i \mu_i n_i \nabla V \cdot \boldsymbol{\nu}
\end{aligned}
\tag{9}
$$

where $a_i = 1$ (cathode-like) if $-\nabla V \cdot \boldsymbol{\nu} > 0$ and $a_i = 0$ (anode like) otherwise

A symmetric argument applies for the electrons. In this case, however, the roles of anode and cathode are inverted, thus

- The anode absorbs electrons, in the sense that any electron, hitting the anode, is captured by it. Thus, the diffusion term of the electrons flux vanishes on its surface, *i.e.*,

$$
\nabla n_e \cdot \boldsymbol{\nu} = 0 \tag{10}
$$

- On the cathode surface, the electrons inward flux is due to thermal and secondary emission, thus

$$
\begin{aligned}
-\mathbf{J_e} \cdot \boldsymbol{\nu} &:= -(\mu_e n_e \nabla V - D_e \nabla n_e) \cdot \boldsymbol{\nu} = \\
&= \gamma_i \mathbf{J_i} \cdot \boldsymbol{\nu} + \frac{1}{4} n_e v_{\text{th}}
\end{aligned}
\tag{11}
$$

where γ_i is the secondary emission coefficient (0.1 in our case) and $v_{\text{th}} = \sqrt{8\kappa_{\text{B}} T / \pi m}$ is the thermal velocity and m is the electron mass.

- As in the case of the ions, the steel chamber behaves differently, depending on the sign of the electric field, *i.e.*,

$$
\begin{aligned}
\mathbf{J_e} \cdot \boldsymbol{\nu} &:= (\mu_e n_e \nabla V - D_e \nabla n_e) \cdot \boldsymbol{\nu} = \\
&= a_e \mu_e n_e \nabla V \cdot \boldsymbol{\nu}
\end{aligned}
\tag{12}
$$

where $a_e = 0$ (cathode-like) if $-\nabla V \cdot \boldsymbol{\nu} > 0$ and $a_e = 1$ (anode like) otherwise

3.1 Final setting of the model

In order to make our result as general as possible, let us define new non dimensional variables $u = V/V_0$ for the potential, $\tilde{n}_i = n_i/n_0$ and $\tilde{n}_e = n_e/n_0$, where V_0 and n_0 are scaling factors to be chosen appropriately. Let us also rescale all the coordinates by the typical length scale of the chamber ($L = 1$ m). Inserting the new variables into Eqs. (1-3) and swapping $\tilde{n}_i$ and $\tilde{n}_e$ with n_i and n_e, respectively, we can set $V_0 = \kappa_{\text{B}} T/e$ ($\sim 10^{-2}$V) and $n_0 = \epsilon\kappa_{\text{B}} T/e^2 L^2$ ($\sim 10^5$m^{-3}). With this notation, we get our final model in non dimensional form as

$$
-\Delta u = n_i - n_e \tag{13}
$$

$$
\nabla \cdot (-n_i \nabla u - \nabla n_i) = \frac{\mu_e}{\mu_i} n_e \tilde{S}(u) \tag{14}
$$

$$
\nabla \cdot \left(n_e \nabla u - \tilde{T}_e \nabla n_e \right) = n_e \tilde{S}(u) \tag{15}
$$

with boundary conditions, in compact form

$$
- [-\mathrm{sgn}(q) n_q \nabla u - \nabla n_q] \cdot \boldsymbol{\nu} =
$$

$$
= \mathrm{sgn}(q)\ a\ n_q \nabla u \cdot \boldsymbol{\nu} + \delta_{qe} \left(\gamma_i \mathbf{J_i} \cdot \boldsymbol{\nu} + \frac{1}{4} n_q v_{\text{th}} \right) \tag{16}
$$

where we have defined a non dimensional electron temperature $\tilde{T}_e = T_e/T$, and we simply set $\tilde{S}(u) = S(V_0 u)$. In the above equations, q indicates the charge carrier, *i.e.*, i or e, and $a = 1$ if $-\mathrm{sgn}(q)\nabla u \cdot \boldsymbol{\nu} > 0$ and $a = 0$ otherwise. The last term starting with the Kronecker delta δ_{qe} applies only to the electrons on "cathode-like" boundary conditions, and is neglected elsewhere.

4 Numerical results

Let us now show some numerical results obtained for some simple configurations of the chamber in 1D and 2D. All the simulations were performed with Comsol® Multiphysics [9], by using a modified convection-diffusion model, for the two current densities, coupled with an electrostatic model (Poisson equation) for the electric potential.

4.1 One dimensional model

In order to be able to interpret correctly the results obtained in 2D, particularly in the configuration with two electrodes, let us start with showing some results obtained in 1D. In this case, our domain is simply a straight line extending between the cathode, on the left, and the anode, on the right. The steel chamber in this case has no particular role and, consequently, the boundary conditions greatly simplify as there is no influence of direction of the electric field on the surface. In spite of this drastic reduction of the model, as we will see, the results already contain an important part of the information given by the 2D case, in more realistic configurations. Let us then start with a plot of the electric potential and electric field norm. In Fig. 3 we represent the non dimensional electric potential u (left) and its spatial derivative u_x, *i.e.*, the electric field (with a positive sign), in logarithmic scale. The electric potential clearly shows two main regimes of the solution. In the first regime corresponding to a region extending between the cathode and the center of the domain, the electric potential grows steeply. Next to this, in a region extending from the center to the other end of the domain, at the anode, the electric potential has already reached its boundary value. However, when we plot the electric field (right), in logarithmic scale, we actually observe a very rich behaviour, showing all the main expected features. First of all, starting from the
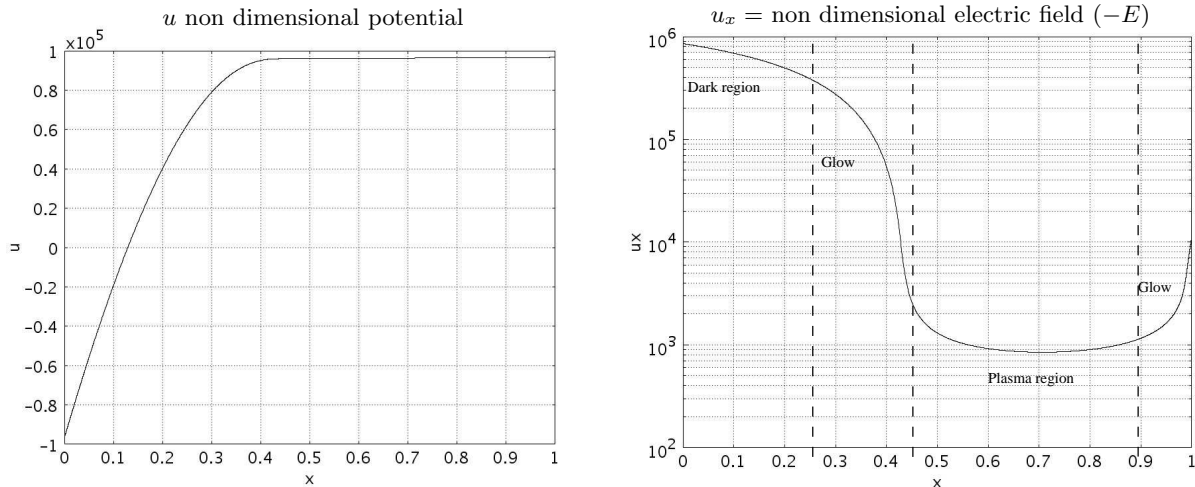
Figure 3: Non dimensional electric potential (left) and norm of the electric field (right). The dimensional potential difference between anode and cathode is set at 5000 V. The norm of the electric field shows clearly the main features expected, such as the "cathode dark space", the negative and positive glow and a plasma region, with low electric field.

cathode (left), the "cathode dark space" extends for roughly one fourth of the domain. The dark space is a region relatively poor of ions (compared to the plasma region), where the charged particles are being accelerated by a strong electric field. In the chamber, this small region appears clearly as a dark space extending all along the cathode. Starting from the right end of the dark space, up to almost a half of the domain, we can observe the "negative glow". In this region, a large number of highly energetic ions (accelerated in the dark space by the electric field), release their energy in form of light. In the experimental setting, one would see a vivid purple zone all around the cathode. Next to the negative glow is a "plasma region". In this region, almost nothing happens, in the sense that, in spite of the large number of charged particles (see Fig. 4), the electric field here is so small that the energy density turns out to be very low. Furthermore, the number of ions and electrons perfectly balance, thus making the plasma region practically neutral (while the cathode dark space and the negative glow are positively charged, Fig. 4-right). The other end of the domain, confined by the anode, is occupied by the positive glow (and the anode dark space). In this region the electric field increases again, although not as much as in the cathode dark space. However, as shown in Fig. 4, in this region, the electrons exceed the ions, making the plasma negatively charged.

The representation of the net charge of the plasma, in Fig. 4-right confirms all our assertions. The cathode dark space, is positively charged, and extends from the cathode up to roughly 0.25. In the negative glow region,

the net charge reaches its maximum and then decreases steeply towards the plasma region, which is neutral as a consequence of the perfect overlapping of the number densities of ions and electrons. Finally, the positive glow shows a negatively charged atmosphere, as the number of electrons exceeds the number of ions in the nearby of the anode. Overall, Fig. 4 shows that the plasma is positively charged as the total number of ions exceeds the total number of electrons, except in the nearby of the anode.

4.2 Two dimensional model − 1 electrode

Let us now show some partial numerical results in the two dimensional model. In order to correlate our results to the previous 1D case, let us assume a simple configuration with one central electrode (cathode), while the steel chamber acts like the anode and is kept at a neutral potential. The cathode is set at a potential (dimensional V) of -3000 V with respect to the steel chamber.

In this simple case (Fig. 5), we can use the cylindrical symmetry of the domain, and reduce the real 3D case to a simpler 2D model. In fact, one can reduce the integration domain to just a half (we chose the lower half) of the vertical section of the chamber, as the upper half is perfectly symmetric to the lower part. The following results were obtained with a FEM triangular mesh (Fig. 5) consisting of 37456 non uniform elements. The system of equations was solved through an affine invariant form of the damped Newton method [9, 10], imple-
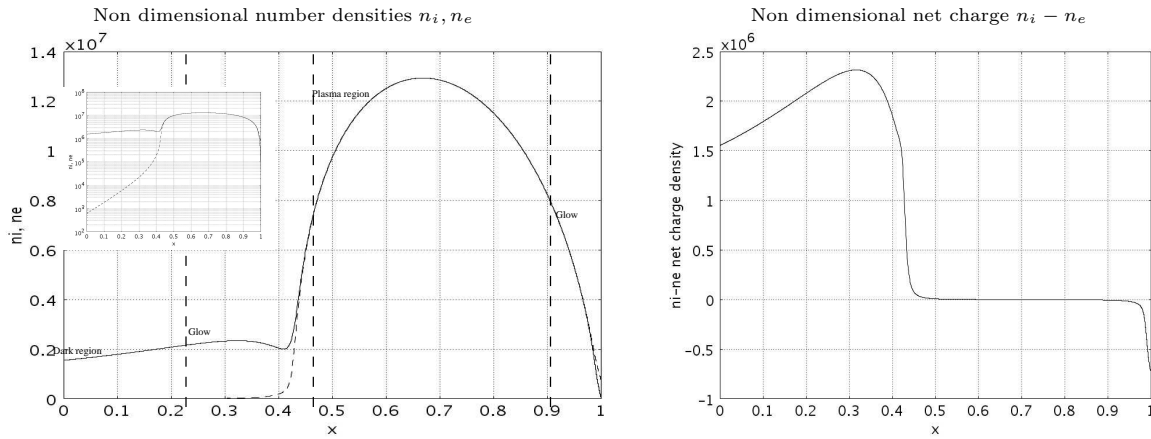
Figure 4: Left: non dimensional number density of ions and electrons (dashed). In the insert, same plot in logarithmic scale. As already shown in the plot of the electric field, the main expected features such as the "cathode dark space", the "negative glow", and the "positive glow" are evident. In the dark space, the number of ions is greatly larger than the number of electrons, but not yet maximum. A maximum is reached in the glow region. The plasma region is neutral, as the number of ions balances exactly the number of electrons (overlapping curves). In the positive glow region, the number of electrons exceeds the number of ions and the plasma in negatively charged. Right: net charge density $\rho = n_i - n_e$. The existence of the four different regions is evident as the net charge density changes drastically from one region to the other.

mented through a direct linear solver UMFPACK [9] included in Comsol® Multiphysics.

As in the previous case, a plot of the non dimensional electric potential (Fig. 6), shows the two main regimes with the potential increasing steeply from the cathode inside the region, and a wide plasma region, where the electric potential has already reached a value which is very close to the one imposed at the anode ($u = 0$ in this case). The similarity between the behaviour of the 1D case and the 2D case with one central electrode is evident when we plot the electric potential evaluated along a horizontal line drawn over the symmetry axis that closes the domain at the top (Fig. 6-right). As in the previous 1D model, the two regimes (actually hiding the four regions already shown in the 1D model) with the potential increasing steeply proceeding from the cathode inwards the integration domain, and the "plasma region" with an almost constant potential, are clearly evident. A similar parallelism between the 1D model and the cylindrically symmetric 2D one is evident when we plot the number densities of ions n_i and electrons n_e (Fig. 7). Again, as in the previous case, the two distributions overlap perfectly in the "plasma region", while near the cathode the number of ions is largely greater than the number of electrons. Viceversa, near the anode (the steel chamber in this case), the electrons exceed the ions, thus making the plasma locally negative, but positive overall. Fig. 7 shows also a clear resemblance with the number density of positive ions and electrons reported by Boeuf in [6]. The main

differences between our case and theirs, besides, possibly, the value of the scaling factors, is due probably due to the different choice of boundary conditions for the potential of the steel chamber (linear in their case, uniform in ours).

4.3 Two dimensional model − two electrodes

Let us now approach the case with the widest industrial interest, as it resembles, although yet in a two dimensional representation, the real plant, in the configuration with two electrodes and an alternate electric field. As the cylindrical symmetry is lost, due to the introduction of the second electrode, none of the possible two dimensional reductions can represent the real three dimensional model. However, a horizontal slice of the three dimensional domain (Fig. 8), as we will see, already gives some useful insights of what happens in the central (in height) area of the electrodes of the full three dimensional case, where we can assume some sort of limited translational invariance. The FEM mesh consisted of 6560 non uniform standard triangular elements. As in the previous cases in one or two dimensions, the 2D model with two electrodes shows the typical expected behaviour. Once again, the plot of the electric potential (contour plot in Fig. 9-left) shows a dominance of the region extending from the anode inwards, where the potential is roughly constant. A plot of the potential evaluated along the orthogonal
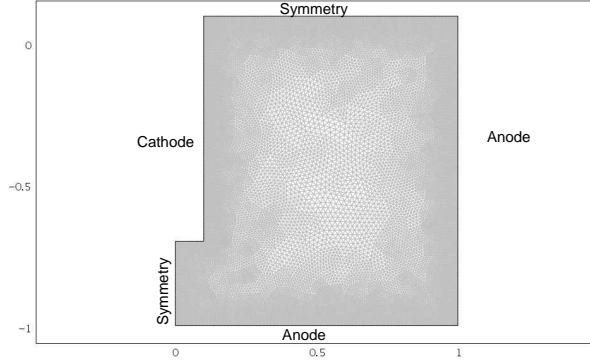
Figure 5: Representation of the two dimensional mesh used in the cylindrically symmetric case with one electrode. The domain is delimited on the left by the cathode, while the steel chamber (bottom and right) constitutes the anode. At the top we impose a symmetry condition as on the central axis.

cross section between the two electrodes (sketched in Fig. 9-left as a horizontal segment between the electrodes) shows that the two-dimensional case resembles accurately the previous 1D and 2D models. As above, the electric potential remains constant in the nearby of the anode and decreases steeply only as we get closer to the cathode. The plot of the norm of the electric field (non dimensional), in Fig. 9-right/bottom, shows again the features already observed in the 1D model, *i.e.*, the dark space, the two glows and the plasma region, although the extension of the regions is now completely different from the previous cases.

In spite of the orthogonality between the two projections (horizontal in this case vs vertical in the cylindrically symmetric one), the great resemblance of this 2D case with the previous cylindrically symmetric model, is clearly evident also when we plot the number density of ions n_i and n_e (Fig. 10). However, in this case, the number density shows some extreme features that were not so evident in the previous cases. Fig. 10-top shows that both the number density of ions (left) and electrons (right) are strongly peaked in the plasma region. In fact, as before, the two peaks are exactly overlapping, as it is evident from the cross section plot of the two densities (bottom-left) and of the net charge $n_i - n_e$ (bottom-right), where we see how, in the plasma region, the net charge is, once again, almost exactly null. As before, the plasma is then positively charged in the cathode dark space and the cathode glow, and negatively charged in the anode glow.

Finally, let us go back for a moment to the boundary conditions imposed in to the steel chamber in Eqs. (9,12). There, we said, we have to impose a different condition, depending on the sign of the electric field on the surface. In other words, we assumed that, some-

how, the steel chamber contributes to the total current crossing the chamber, behaving, in some parts, anode-like, and in others, cathode-like. An insight of this effect, which is clearly rather weak, but yet present, can be obtained by showing a plot of the stream lines of the current density of ions J_i. Fig. 11 shows, as expected, that the ions flux (and similarly the electrons flux, not shown) is concentrated within the region between the electrodes. However, some (non negligible) density is flowing also in the area around the two electrodes, between the electrodes and the steel chamber. There, the electric field streamlines close between the electrodes and the steel chamber. In other words, the steel chamber, through a partial coupling with the electrodes, contributes to the flow of electric current. In particular, the steel chamber behaves like an anode in the area where the streamlines connect it to the cathode, while it behaves like a cathode, where the streamlines connect it to the anode (most of the surface in this case). As mentioned, the contribution of this partial coupling to the total amount of current is fairly low. However, this contribution exists and confirms that the boundary conditions must include it somehow. Furthermore, this suggests that also a coupling of different nature, for instance, due to residual capacity effects, is possible between the steel chamber and the electrodes. This type of coupling was completely neglected in our case, since we assumed a static field, however, this result shows that, in case of alternate current, it could contribute even further to the passage of electric current through the plant.
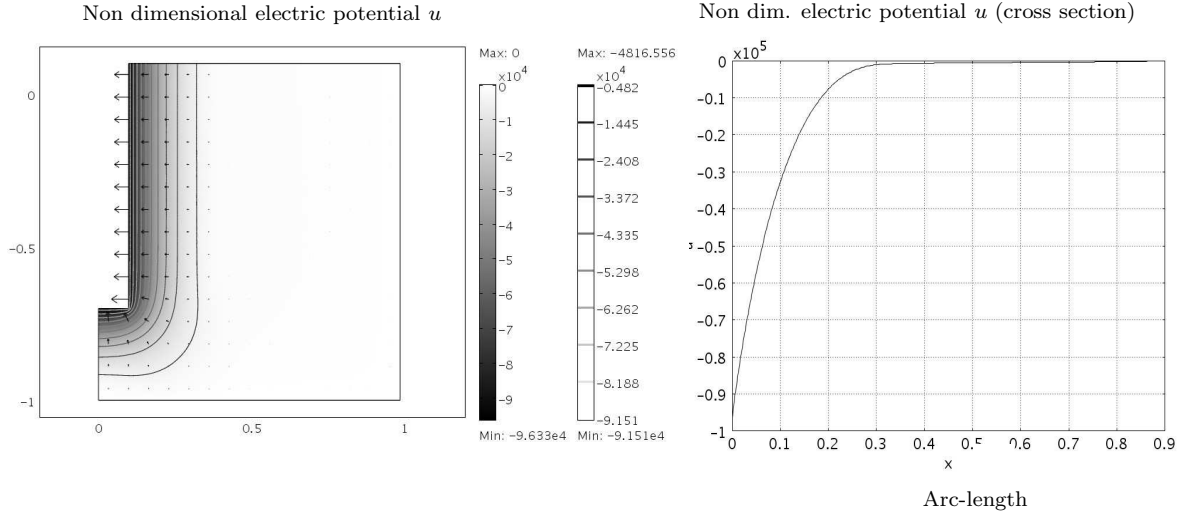
10

Figure 6: Left: Representation of the non dimensional electric potential u in the two-dimensional case with one central electrode. The potential increases steeply from the cathode into the domain, reaching quickly a value already close to the one imposed at the anode $u = 0$. The arrows pointing inwards the cathode show the strength of the electric field in that area, compared to the plasma region, where they are invisible as the electric field is low. Right: Cross section obtained by drawing a horizontal line at the top of the domain, *i.e.*, on the horizontal symmetry axis. The plot shows the perfect correspondence of this case, to the 1D case.

5 Conclusions

We analyzed the behaviour of plasma atmosphere in a PVD industrial plant by means of a mathematical model involving the electric potential and the number density of ions and electrons. The drastic simplifications we made in setting the mathematical model, allowed us to solve it numerically in a fairly straightforward way. The main difficulty of the model, as already mentioned in the literature, concerns the setting of the boundary conditions. In fact, previous results show that the usual Neumann or Dirichlet boundary conditions are too simple to give physically meaningful results. For this reason, we made an intermediate choice of mixed boundary conditions, that take into account of, at least, secondary and thermal emission of electrons. However, as in our case the plant configuration consists of two electrodes and the steel chamber, the boundary conditions turn out to depend on the solution inside the domain. The three equations of the model are therefore coupled in a strongly non linear way. In spite of this, for fairly simple geometries, such as the shown two dimensional cut, and the corresponding full three dimensional case (not included), the numerical solution of the model is still possible. In fact, the two dimensional model with two electrodes show a great resemblance with the one dimensional case and the cylindrically symmetric two dimensional case. The three analyzed cases show a similar behaviour of the electric potential, with evidence of two different regimes. A plasma region is clearly evident with almost constant potential, bounded by the anode. A highly energetic glow region with the potential increasing steeply, extends between the plasma and the cathode.

Similar considerations can be made, concerning the number densities of ions and electrons. In all the shown cases (and similarly it happens in the three dimensional case, although that is rather more difficult to visualize) the number density of ions and electrons overlap almost exactly in the plasma region. In the cathode dark space and positive glow, the ions greatly dominate, while in the negative glow (close to the anode), the number of electrons exceeds the number of ions. This behaviour was again expected, since it was both observed experimentally and simulated by a mathematical model for the one dimensional case (such as the glass tube [8]) and some simple configurations of the 2D model [6]. As far as we know, this is the first case where a full two-dimensional model, with no rotation invariance, is solved numerically and fully reported. Furthermore, as far as we know, it is the first time that a clear comparison between the 1D model and more complex 2D models, either with one or two electrodes, is made. Clearly, this is not conclusive, as the full three dimensional was not analyzed in detail. However, it is the first time that a published numerical model actually takes into the account of the real industrial configuration of an alternate current (AC) plant.

In terms of the application of our results in an in-

Non dimensional ions number density n_i Non dimensional electrons number density n_e
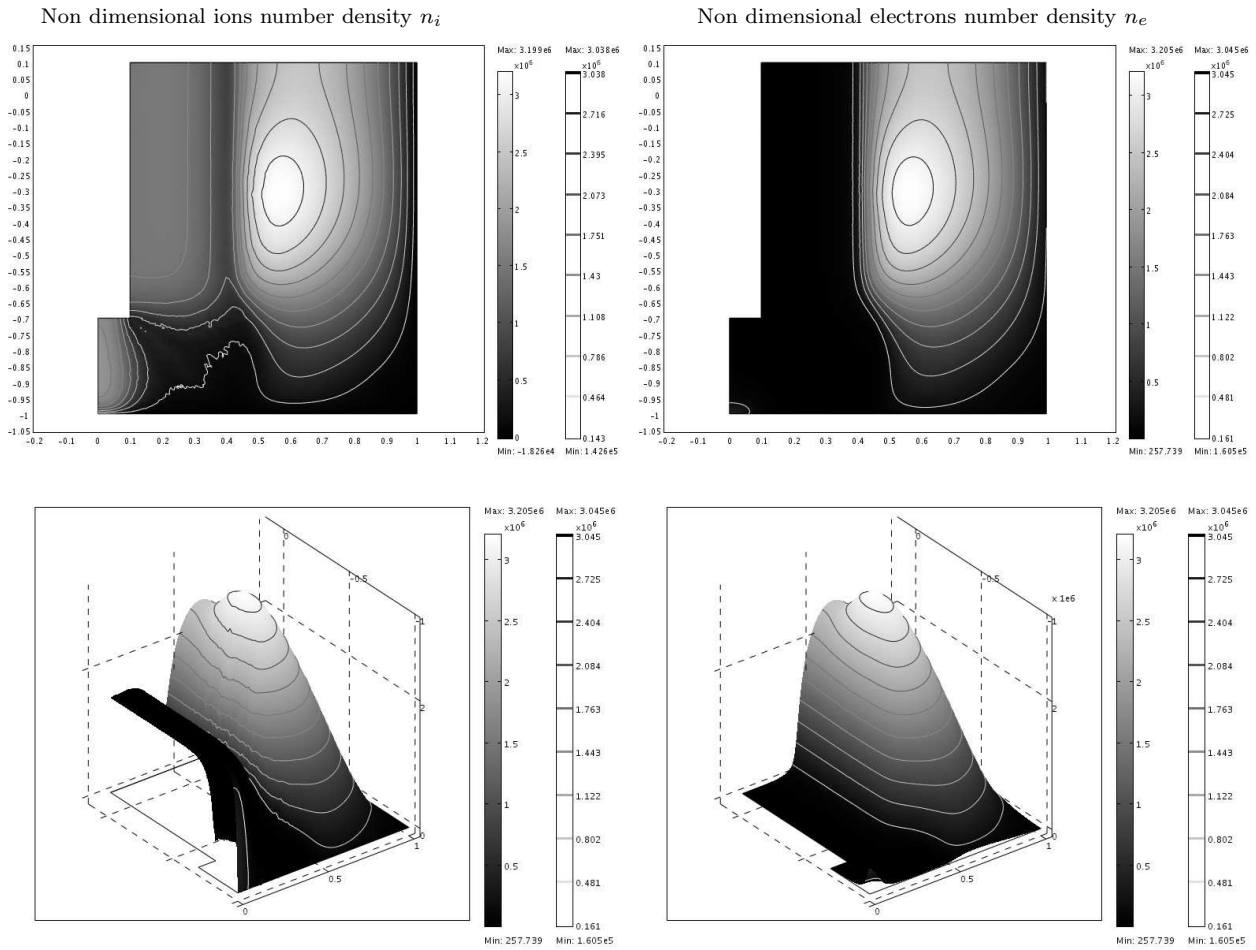

Figure 7: Left: Contour plot (top) and 3D surface (bottom) of the non dimensional number density of ions (top). Right: Contour plot (top) and 3D surface (bottom) of the non dimensional number density of electrons. As in the 1D model, the two distributions overlap perfectly in the central area (plasma region) of the domain. Near the cathode (dark space and glow) the number of ions largely exceeds the number of electrons, thus making the plasma overall, positively charged.

dustrial contest, one should try to correlate these theoretical considerations with some experimental results of the deposition process, in order to show the influence of the different conditions of the plasma on the polymeric film formed. Clearly, only partial considerations can be made by a discussion of our numerical results. One expects, for instance, the plasma region to be fairly quiet, in terms of electric energy, as in spite of the great number of charged particles (both ions and electrons reach their absolute maximum in the plasma region), the electric field is almost null. Conversely, in the negative glow region, a large number of ions (compared to the electrons) are strongly accelerated by a strong electric field. This is the most energetic region of the whole domain, and one expects a rather dramatic behaviour of the plasma. For example, in the glow region (or the cathode dark space), one expects a strong

"sputtering effect" due to the ions hitting the surface of substrate to be treated and, possibly, removing the aluminium film. That is clearly a phenomenon that one would want to avoid as much as possible, when choosing where to pose the pieces to be treated within the chamber. However, at this stage, *i.e.*, without a systematic experimental campaign it is hard to give any further interpretation of the model, except for very general considerations, concerning the real industrial process of polymerization and coatings. In spite of this, we believe our model can be a good starting point for a systematic investigation of the real process. In order to interpret correctly our results and guide the industrial process, one should, possibly, not only compare them with experiments and direct observations, but also with the results of a simplified polymerization model. One could then correlate the results from the two models
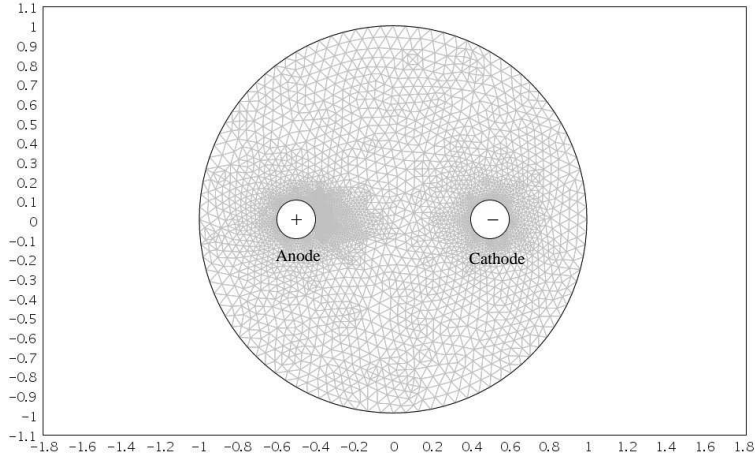
Figure 8: Representation of the mesh used to solve the model in the two dimensional case, obtained by cutting horizontally the original 3D domain. The two cylindrical electrodes are represented by two circles, the anode on the left, and the cathode on the right.

with observations, and draw some conclusions about the real process of coating. For instance, a deeper investigation of the polymerization process could suggest that a highly energetic region is favorable in terms of speed and effectiveness of the polymerization.

Although this project of investigation is just at the beginning, we believe that our model marked a good step forward in the direction of a more systematic and scientific approach to the optimization of a commonly used, but not yet fully understood, industrial process.

References

[1] J E Allen. A note on the generalized sheath criterion. *Journal of Physics D: Applied Physics*, 9(16):2331, 1976.

[2] J G Andrews and P G Stangeby. Generalization of the sheath criterion in an anisotropic plasma. *Journal of Physics A: General Physics*, 3(5):L39, 1970.

[3] Michael S. Barnes, Tina J. Cotler, and Michael E. Elta. Large-signal time-domain modeling of low-pressure rf glow discharges. *Journal of Applied Physics*, 61(1):81–89, 1987.

[4] J.-P. Boeuf. Numerical model of rf glow discharges. *Phys. Rev. A*, 36(6):2782–2792, Sep 1987.

[5] J P Boeuf and L C Pitchford. Two-dimensional model of capacitively coupled rf discharge and comparisons with experiments in the gaseous electronics conference reference reactor. *Phys. Rev. E*, 51(2):1376–1390, 1995.

[6] J.P. Boeuf. A two-dimensional model of dc glow discharges. *Journal of Applied Physics*, 63:1342, 1988.

[7] D Bohm. In A Guthrie and R K Wakerling, editors, *The characteristics of electrical discharges in magnetic fields*, page 77. McGraw-Hill, New York, 1949.

[8] W H Class. Basics of plasmas. Internal notes by Materials Research Corporation.

[9] AB Comsol. COMSOL multiphysics users guide. *Version: September*, 2005.

[10] P. Deuflhard. A modified Newton method for the solution of ill-conditioned systems of nonlinear equations with application to multiple shooting. *Numerische Mathematik*, 22(4):289–315, 1974.

[11] A. Fiala, LC Pitchford, and JP Boeuf. Two-dimensional, hybrid model of low-pressure glow
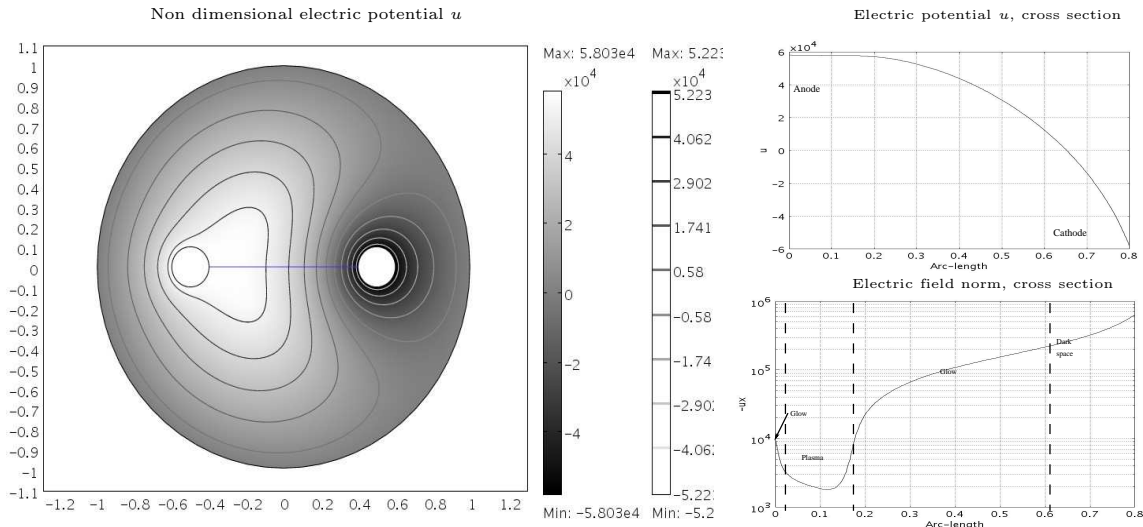
Figure 9: Non dimensional potential u in contour plot (left) and along the cross section between the electrodes sketched as the horizontal segment between the electrodes (right/top). Both representations of the potential show the dominance of the area at positive potential, bounded by the anode, compared to the area at negative potential bounded by the cathode. Right/bottom, non dimensional electric field (norm) along the same cross section as above. The electric field shows again the typical features as the previous cases, such as the dark space, the positive and negative glows, and the plasma region.

discharges. *Physical Review E*, 49(6):5607–5622, 1994.

[12] R. N. Franklin and J. R. Ockendon. Asymptotic matching of plasma and sheath in an active low pressure discharge. *Journal of Plasma Physics*, 4(02):371–385, 1970.

[13] V. Godyak and N. Sternberg. On the consistency of the collisionless sheath model. *Physics of Plasmas*, 9:4427, 2002.

[14] Evangelos Gogolides, Jean-Philippe Nicolai, and Herbert H. Sawin. Comparison of experimental measurements and model predictions for radio-frequency ar and sf[sub 6] discharges. *Journal of Vacuum Science & Technology A: Vacuum, Surfaces, and Films*, 7(3):1001–1006, 1989.

[15] D.B. Graves. Fluid model simulations of a 13.56-MHz rf discharge: Time and space dependence of rates of electron impact excitation. *Journal of Applied Physics*, 62:88, 1987.

[16] D.B. Graves and K.F. Jensen. A continuum model of DC and RF discharges. *IEEE Transactions on Plasma Science*, 14(2):78–91, 1986.

[17] S. Guo and WJ van Ooij. Kinetics of DC Discharge Plasma Polymerization of Hexamethyldisiloxane

and Pyrrole. *Plasmas and Polymers*, 3(1):1–21, 1998.

[18] G. J. M. Hagelaar, F. J. de Hoog, and G. M. W. Kroesen. Boundary conditions in fluid models of gas discharges. *Phys. Rev. E*, 62(1):1452–1454, Jul 2000.

[19] D Hegemann, U Schutz, and A Fischer. Macroscopic plasma-chemical approach to plasma polymerization of HMDSO and CH_4. *Surface & coatiny technology*, 20:458–462, 2005.

[20] M. Meyyappan and JP Kreskovsky. Glow discharge simulation through solutions to the moments of the Boltzmann transport equation. *Journal of Applied Physics*, 68:1506, 1990.

[21] C J Mojab. Glow discharge processes, by brian chapman. *Journal of Vacuum Science and Technology*, 19(3):812–812, 1981.

[22] H. Muta, M. Koga, N. Itagaki, and Y. Kawai. Numerical investigation of a low-electron-temperature ECR plasma in Ar/N2 mixtures. *Surface & Coatings Technology*, 171(1-3):157–161, 2002.

Non dimensional ions number density n_i

Non dimensional electrons number density n_e

Non dimensional number densities n_i and n_e

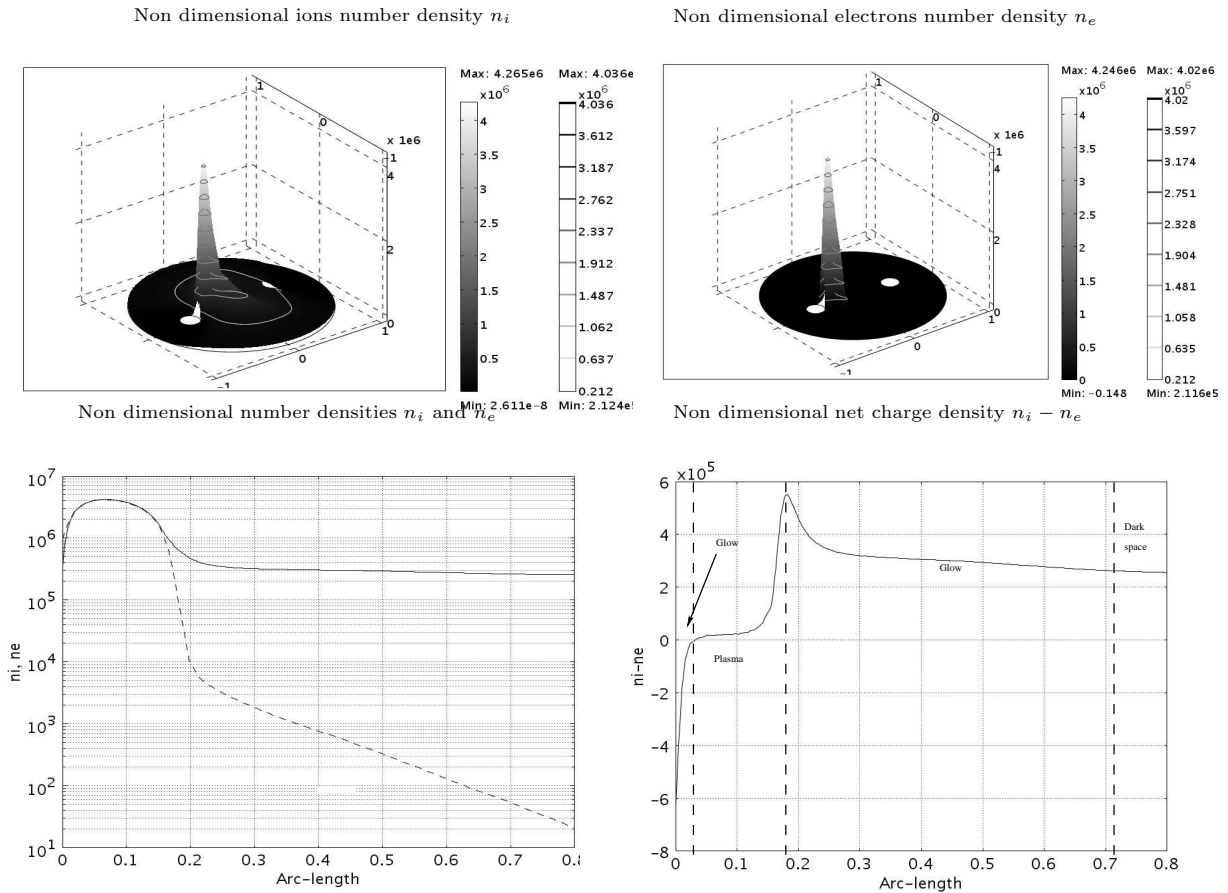Non dimensional net charge density $n_i - n_e$

Figure 10: Non dimensional density of ions (top/left) and electrons (top/right) in three dimensional representation. The two distributions are strongly peaked in the plasma region. However, the two peaks overlap almost exactly, as clear from the cross section plot (bottom/left) and from the cross section plot of the net charge density $n_i - n_e$ (bottom/right). The net charge density (bottom/right) shows also the typical behaviour encountered in the previous cases. The plasma region is roughly neutral, while the cathode dark space and the negative glow are positively charged. The positive glow is negatively charged, as the number of electrons exceeds the number of ions.

[23] JDP Passchier and WJ Goedheer. A two-dimensional fluid model for an argon rf discharge. *Journal of Applied Physics*, 74:3744, 1993.

[24] D.Q. Posin. The Townsend Coefficients and Spark Discharge. *Physical Review*, 50(7):650–658, 1936.

[25] AD Richards, BE Thompson, and HH Sawin. Continuum modeling of argon radio frequency glow discharges. *Applied physics letters*, 50(9):492–494, 1987.

[26] K.U. Riemann. The Bohm criterion and sheath formation. *Journal of Physics D: Applied Physics*, 24:493–518, 1991.

[27] K.U. Riemann. The influence of collisions on the plasma sheath transition. *Physics of plasmas*, 4:4158, 1997.

[28] S. Roy, BP Pandey, J. Poggie, and D.V. Gaitonde. Modeling low pressure collisional plasma sheath with space-charge effect. *Physics of Plasmas*, 10:2578, 2003.

[29] F.H. Sanders. The Value of the Townsend Coefficient for Ionization by Collision at Large Plate Distances and Near Atmospheric Pressure. *Physical Review*, 41(5):667–677, 1932.

[30] F.H. Sanders. Measurement of the Townsend Coefficients for Ionization by Collision. *Physical Review*, 44(12):1020–1024, 1933.

[31] J. T. Scheuer and G. A. Emmert. A collisional model of the plasma presheath. *Physics of Fluids*, 31(6):1748–1756, 1988.
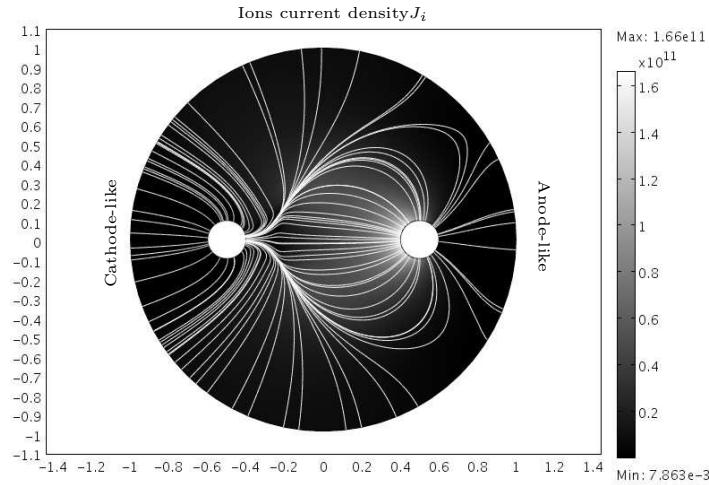
Figure 11: Ions density flux J_i and streamlines of the electric field. The current flows, as expected, mainly between the two electrodes, with a high density of ions flux in the vicinity of the cathode. However, some electric field streamlines close up on the steel chamber. The steel chamber therefore contributes to the total current flow within the chamber, due to a partial coupling between the electrodes and the chamber itself. In the area where the streamlines connect the chamber to the anode, the chamber behaves like a cathode, while in the area where the streamlines connect to the cathode, the chamber behaves like the anode.

[32] TE Sheridan and J. Goree. Collisional plasma sheath model. *Physics of Fluids B: Plasma Physics*, 3:2796, 1991.

[33] M. Surendra, D. B. Graves, and G. M. Jellum. Self-consistent model of a direct-current glow discharge: Treatment of fast electrons. *Phys. Rev. A*, 41(2):1112–1125, Jan 1990.

[34] L Tonks and I Langmuir. A general theory of the plasma of an arc. *Phys. Rev.*, 34(6):876–922, Sep 1929.

[35] J. Townsend. *Electricity in gases*. Clarendon Press, 1915.

[36] H.-B. Valentini. Bohm criterion for the collisional sheath. *Physics of Plasmas*, 3(4):1459–1461, 1996.

[37] H-B Valentini. Sheath formation in low-pressure discharges. *Plasma Sources Science and Technology*, 9(4):574, 2000.

[38] S.B. Wang and A.E. Wendt. Sheath thickness evaluation for collisionless or weakly collisional bounded plasmas. *IEEE Transactions on Plasma Science*, 27(5):1358–1365, 1999.

[39] AL Ward. Calculations of Cathode-Fall Characteristics. *Journal of Applied Physics*, 33:2789, 2004.

[40] E Zawaideh, F Najmabadi, and R W Conn. Generalized fluid equations for parallel transport in collisional to weakly collisional plasmas. *Physics of Fluids*, 29(2):463–474, 1986.